Available online at www.sciencedirect.com

SciVerse ScienceDirect

Ceramics International 39 (2013) 2619–2629

CERAMICS INTERNATIONAL

www.elsevier.com/locate/ceramint

# Titanium dioxide modified with transition metals and rare earth elements: Phase composition, optical properties, and photocatalytic activity

D.M. Tobaldi[a,*], A. Sever Škapin[b], R.C. Pullar[a], M.P. Seabra[a], J.A. Labrincha[a]

[a]*Materials and Ceramics Engineering Department/CICECO, University of Aveiro, Campus Universitário de Santiago, 3810-193 Aveiro, Portugal*
[b]*Slovenian National Building and Civil Engineering Institute, Dimičeva 12, SI-1000 Ljubljana, Slovenia*

Received 28 August 2012; received in revised form 4 September 2012; accepted 7 September 2012
Available online 15 September 2012

**Abstract**

A series of titania–transition metal and titania–rare earth element mixtures, with the stoichiometry $Ti_{1-x}M_xO_2$, where $M$=Ce, Eu, La, Nb, W, Y, and $x$ ranging from 0 to 0.05 atoms per formula unit, were prepared via solid-state reaction of the precursor oxides. The products of the synthesis were thermally treated in air and two maximum temperatures (900 and 1000 °C) were reached.

The addition of transition metal and rare earth ions to the $TiO_2$ structure modified the anatase-to-rutile phase transition temperature, depending on the valence state of the ions added. Transition metals entered the titania structure, but essentially no solid solution between the rare earth elements and $TiO_2$ was detected.

The photocatalytic activity of the powders was assessed in liquid–solid and gas–solid phases, under UVA and visible-light irradiation, monitoring the degradation of an organic dye and isopropanol, respectively. The results were explained by taking into account the relative amounts of anatase and rutile in the samples, the specific surface area of the powders, and their optical properties.


*Keywords:* A. Powders: solid state reaction; D. $TiO_2$; E. Functional applications; Photocatalysis

## 1. Introduction

Titanium dioxide ($TiO_2$) is a very common material used in everyday life applications. In recent decades, $TiO_2$ rose as the most popular material for photocatalytic applications—outdoor and indoor air purification [1–3] or decontamination of polluted waters [4]. Photocatalysis is the phenomenon in which a substance, the photocatalyst, modifies the rate of a reaction, via the action of light having a suitable wavelength; semiconductors are such substances [5,6]. When a semiconductor is irradiated with photons having energy higher than or equal to its energy band gap ($E_g$), an electron ($e^-$) is able to migrate from the valence band to the conduction band, leaving a hole ($h^+$) behind. Such a photo-generated couple ($e^-$–$h^+$) is able to reduce and/or oxidise a pollutant adsorbed on the photocatalyst surface [7]. $TiO_2$ – mainly in its anatase and rutile crystallographic polymorphs – is one of the most appreciated semiconductor photocatalysts. The positive features of heterogeneous photocatalysis with it, are: the reactions take place at mild operating conditions (low level of solar or artificial illumination, room temperature (RT), and atmospheric pressure); no chemical additive is necessary; the likely intermediates of the reactions are not dangerous or, at least, less dangerous than the original pollutant [8]; even very recalcitrant and persistent pollutants may be degraded [9]. Moreover, $TiO_2$ is also a relatively low-cost product, as well as non toxic.

Being a wide band gap semiconductor material ($E_g$=3.2 and 3.0 eV for anatase and rutile, respectively), the photocatalytic reaction of $TiO_2$ is activated by UVA light, although titania is transparent for most of the visible radiation region. This means that the photocatalytic reaction is exploited by only 3–5% of the solar spectrum. A number of attempts have been made to overcome this negative aspect. One of the routes followed, with the aim

*Corresponding author. Tel.: +351 234 370 041.
*E-mail address:* david.tobaldi@ua.pt (D.M. Tobaldi).

0272-8842/$ - see front matter © 2012 Elsevier Ltd and Techna Group S.r.l. All rights reserved.
http://dx.doi.org/10.1016/j.ceramint.2012.09.027

of extending the spectral response of pure titania to visible-light, was modifying its electronic structure by the insertion of non-metal atoms [10–14], transition metal (TM) ions [15,16], or rare earth elements (REE) [17,18]. The addition of dopants – such as anions, TMs, or REEs – into the $TiO_2$ lattice should produce a narrowing of the band gap, or an introduction of mid-states in the titania band gap, resulting in an absorption toward the visible region of the spectrum [14]. The non-metal doping often had a detrimental effect on the photocatalytic activity of $TiO_2$ under UVA exposure, because of an enhancement of charge recombination [19]; moreover, anion-doped titania also showed a low thermal and chemical stability [20]. Therefore, the use of suitable dopants (at a suitable concentration) such as TM or REE ions, should improve the photocatalytic performances of $TiO_2$, when thermally treated at high temperatures.

The present work deals with an investigation of $TiO_2$ modified with TMs ($Nb_2O_5$ and $WO_3$) and REEs ($CeO_2$, $Eu_2O_3$, $La_2O_3$, and $Y_2O_3$). The modification that TMs and REEs would exert on titania – anatase-to-rutile phase transition (ART) temperature, morphology, microstructure, and optical properties – were taken into account, in order to fully describe the modified titania powders, and their photocatalytic activity under UVA, and visible-light irradiation. Furthermore, the $TiO_2$–TM and $TiO_2$–REE mixtures were fired at high temperature (900 and 1000 °C), with the purpose of checking whether the photocatalytic activity was retained at such temperatures. Consequently, the studied mixtures may be employed on the surface of materials that need treatments at high temperature, so as to give them an innovative surface functionalisation [21,22].

## 2. Experimental

### 2.1. Sample preparation

The powders were prepared via solid-state reaction of the two crystalline end-members, according to this stoichiometry: $Ti_{1-x}M_xO_2$ where $M$ = Ce, Eu, La, Nb, W, and Y. For the REE addition ($CeO_2$, $Eu_2O_3$, $La_2O_3$, and $Y_2O_3$) $x = 0$, 0.01 and 0.025 atoms per formula unit (apfu), whilst for TM addition ($Nb_2O_5$ and $WO_3$), $x$ was equal to 0, 0.01, 0.025, and 0.05 apfu. Aeroxide P25 $TiO_2$ powder was used as the titania source (hereafter designated as D), while reagent-grade $CeO_2$, $Eu_2O_3$, $La_2O_3$, $Nb_2O_5$, $WO_3$, and $Y_2O_3$ (all supplied by Aldrich) were used as TM and REE precursors. Powders were admixed and wet ground in a rotary ball mill (30 min with deionised water and zirconia sintered balls). Mixtures were dried in an oven (105 °C overnight), ground in an agate mortar, and then calcined; the firing was performed in an electric oven with static air atmosphere, the heating rate was 200 °C $h^{-1}$, and two maximum temperatures were reached (900 and 1000 °C), with a soaking time at the maximum temperature of 4 h, followed by natural cooling. $TiO_2$ samples, used as reference, were referred to as the first initial of the commercial powder used, followed by a number indicative of the maximum firing temperature reached (i.e. D-900 for Aeroxide P25 $TiO_2$ powder fired at 900 °C); in case of $TiO_2$–TM or $TiO_2$–REE mixtures, the symbol of the chemical element followed by the amount of apfu inserted was used (i.e. sample with 0.01 apfu of Europium added to Aeroxide's titania, and calcined at 900 °C, is referred to as: Eu0.01-900).

### 2.2. Sample characterisation

The phase composition of the starting titania powders, as well as of the $TiO_2$–TM and $TiO_2$–REE mixtures, was obtained via X-ray diffraction, using a Rigaku Geigerflex (JP); the patterns were collected in the 15–80° 2θ range (0.02° 2θ $s^{-1}$ step-scan and 5 s/ step). The anatase/rutile relative amounts in the titania reference powders, as well as in the modified samples that were composed only of anatase and rutile, were calculated using the Spurr–Myers procedure [23]. Instead, a semi-quantitative estimate of the likely amount of anatase/rutile ratio, as well as the secondary phases – in the $TiO_2$–TM and $TiO_2$–REE mixtures – was achieved by adopting the generalised RIR method [24]. In both cases, we assumed the absence of amorphous phase in the examined powders.

The morphology of the samples was investigated by SEM (Hitachi SU-70, JP), equipped with an energy dispersive X-ray spectroscopy (EDS) attachment (Bruker AXS, DE). Optical spectra of the samples – and subsequently, the $E_g$ – were acquired on a Shimadzu UV 3100 (JP), in the UV–Vis range (200–800 nm), with 0.02 nm step-size, and using $BaSO_4$ as reference. The diffuse reflectance was converted into the absorption coefficient α, using the Kubelka–Munk function [25]:

$$\alpha \approx \frac{K}{S} = \frac{(1-R_\infty)^2}{2R_\infty} \equiv F(R_\infty) \quad (1)$$

The $E_g$ of the powders was calculated using the differential reflectance method: plotting the first derivative of reflectance versus the wavelength $\lambda$ ($dR/d\lambda$), the maximum value of such plot corresponds to the band gap of the semiconductor material [26]. The specific surface area (SSA) of the prepared samples was evaluated by the Brunauer–Emmett–Teller method (BET) (Micromeritics Gemini 2380, US) using $N_2$ as the adsorbate gas.

### 2.3. Evaluation of photocatalytic activity

The photocatalytic activity of the prepared powders was evaluated both in liquid–solid phase and in gas–solid phase, the former monitoring the degradation of an organic dye – methylene blue (MB) – via a spectrometer (Shimadzu UV 3100, JP), the latter monitoring the degradation of isopropanol, and the subsequent formation of acetone, by FT–IR spectroscopy.

The liquid–solid phase tests were performed at RT in a cylindrical photocatalytic reactor containing a water solution of the dye (1 L), at the initial concentration of 5 mg $L^{-1}$. The concentration of the photocatalyst in the slurry was 0.25 g $L^{-1}$. In order to mix the solution thoroughly, the slurry was stirred throughout the reaction; the reactor was covered with a watch-glass, so as to avoid the evaporation of the solution. The lightning of the reacting system was achieved by two lamps placed at the side of the reactor, and the distance between the lamps and the reactor was 5 cm. The UVA-light source was a germicidal lamp (Philips PL-S 9 W, NL), having an irradiance of approximately 13 W $m^{-2}$ in the UVA range; while the visible-light source was a fluorescent lamp (Philips master PL-S 2 P 9 W/840, NL), with an irradiance of ~50 W $m^{-2}$ in the visible region and $600 \times 10^{-3}$ W $m^{-2}$ in the UVA region. In the experiments, the photocatalytic degradation of MB was monitored by sampling from the reactor, at regular time intervals, 4 mL of the slurry. The powders in the samples were separated by centrifugation, and then the MB concentration in the liquid was determined by measuring the absorbance in a spectrophotometer at a wavelength of 665 nm. The extent of MB photocatalytic degradation $\xi$, was evaluated as

$$\xi\% = \frac{C_0 - C_s}{C_0} \times 100 \quad (2)$$

where $C_0$ is the initial MB concentration and $C_S$ is the concentration after a certain UVA/visible irradiation time. Control experiments (i.e. photolysis of the MB dye), under direct UVA and visible-light irradiation, were performed prior to testing the photocatalytic activity of the prepared samples. The photocatalytic reaction is a pseudo first-order reaction, hence the apparent first-order constant ($k'_{app}$) can be evaluated as

$$\ln\left(\frac{C_0}{C}\right) = k'_{app} t \quad (3)$$

where $C_0$ is the initial concentration of MB and $C$ is its concentration after a certain irradiation time $t$. Therefore, the plot of $\ln(C_0/C)$ Vs the irradiation time $t$, gives a straight line, whose slope corresponds to the value of the pseudo first-order apparent rate constant ($k'_{app}$) [27]. The total irradiation time, in the liquid–solid phase reaction, was set at 7 h, and the lights were turned on 30 min after having put the photocatalyst in the reacting system, in order to allow the adsorption/desorption of the dye onto the powders.

The device employed for the gas–solid phase tests, was a cylindrical reactor (1.4 L in volume), covered by quartz glass connected by Teflon tubes to the FT–IR spectrometer, and the whole system was hermetically sealed. The principle of the method is presented in detail elsewhere [28,29]. The light source was a 300 W Xenon lamp (Newport Oriel Instruments, US), having light intensity of approximately 30 W $m^{-2}$ in the $\lambda$ range of 300–400 nm, and 300 W $m^{-2}$ in the $\lambda$ range of 400–800 nm. Visible-light irradiation was achieved by way of a filter at 400 nm; light intensity was approximately zero in the $\lambda$ range of 300–400 nm and 160 W $m^{-2}$ in the $\lambda$ range of 400–800 nm. The samples were prepared in the form of a thin layer of powder, with a constant mass (about 50 mg), and thus approximately constant thickness, in a petri dish having 6 cm in diameter; the working distance between the petri dish and the lamp was 6 cm. The relative humidity in the reacting system was kept constant in the range 25–30%, by means of a flow of air passing through molecular sieves, until a pre-defined humidity was attained. Each experiment was performed by injecting 3 μL of isopropanol (~700 ppm in gas phase) into the reacting system through a septum; the total reaction time was set at 24 h, and the lamp was turned on after a certain period of time – after isopropanol injection – in order to allow an equilibration of isopropanol adsorption onto the powder. The isopropanol degradation, as well as the acetone formation-degradation process, were followed by monitoring the calculated area of their characteristic peaks at 951 $cm^{-1}$ and 1207 $cm^{-1}$, respectively, by using a FT–IR spectrometer (Perkin Elmer Spectrum BX, US). The photocatalytic activity was evaluated as the rate constant of the initial acetone formation, because at RT, the photocatalytic oxidation of isopropanol to form acetone is fast, whereas the subsequent oxidation of acetone to $CO_2$ and $H_2O$ is slower [30]. Acetone formation is characteristic, and distinguished from the subsequent photo-oxidation. The accuracy of the method we used was estimated to be 0.5 ppm $h^{-1}$.

## 3. Results and discussion

### 3.1. X-ray diffraction: transition metal ions addition

The characteristics of the starting titania powder are depicted in Table 1 and Fig. 1a. Sample D (Aeroxide P25 powder) is a mixture of anatase and rutile (86.4 wt% and 13.6 wt%, respectively), and possesses a high specific surface area (52.5 $m^2$ $g^{-1}$). It consists of strongly agglomerated nanometric particles, sub-spherical in shape, as showed in Fig. 1a. At 900 °C, it completes the ART; its high surface

Table 1
Phase composition, energy band gap, and specific surface area of the starting titania powder.

| Sample | Phase composition (wt%) | | $E_g$ (eV) | | $S_{BET}$ ($m^2g^{-1}$) |
|---|---|---|---|---|---|
| | Anatase | Rutile | Anatase | Rutile | |
| Degussa P25 | 86.4 | 13.6 | 3.30 ± 0.01 | 3.11 ± 0.01 | 52.5 |

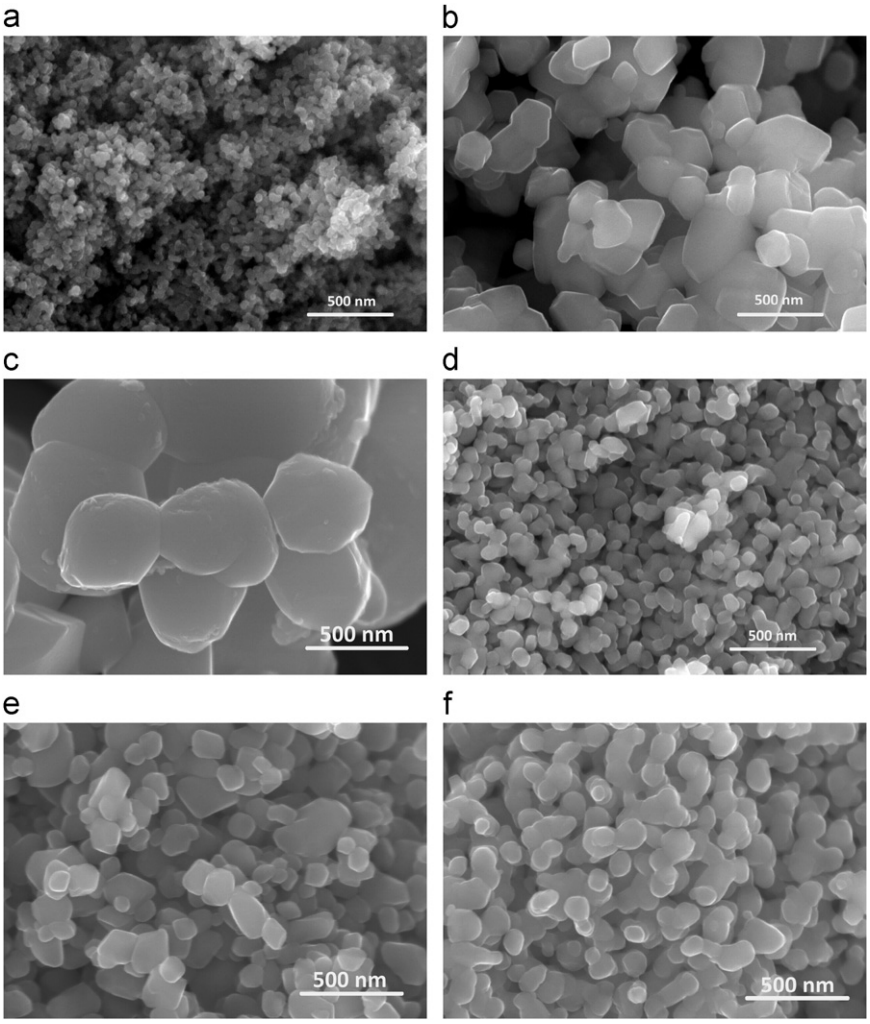


Fig. 1. SEM micrographs of: (a) sample D (Degussa P25 powder at RT), (b) sample D-900, (c) sample D-1000, (d) sample W0.01-900, (e) sample W0.01-1000, and (f) sample La0.01-900.

area encouraged the nucleation-growth phenomenon, and hence promoted the ART [31] (Fig. 1b). As can be seen in Fig. 1a–b, the thermal treatment, from RT to 900 °C, encourages a partial sintering of the starting titania powder. At 1000 °C, the densification becomes more evident, the particles are coarsening, and there is an initial growth of inter-particle necks (Fig. 1c).

The addition of $WO_3$ to titania, delayed the ART, in all the three compositions, there is still a certain amount of anatase. $WO_3$ addition also limited the decrease of SSA, compared to the sample D-900 (Table 2). Compared to the reference sample, that was thermally treated at 900 °C (Fig. 1a), the doping with $WO_3$ (Fig. 1d) caused a decrease in the particle size growth, even if a certain degree of densification was already evident. Actually, the ART is delayed by the insertion of cations having valence $>4+$, because of the reduction of the oxygen vacancies, and forming interstitial $Ti^{3+}$, hence repressing the atomic transfer in the anatase structure [32]. At this temperature (900 °C), we can assume that, with an addition of tungsten equal to 0.01 apfu, a solid solution between $TiO_2$ and $WO_3$ happened (1.3 wt% of anatase and 98.7 wt% of rutile, refer to Table 2), the effective ionic radii of $^{[6]}W^{4+}$ and $^{[6]}Ti^{4+}$ being 0.66 and 0.61 Å, respectively [33]. Higher additions of $WO_3$ (0.025 and 0.05 apfu) led to a higher presence of anatase, but they also led to the formation of an excess of $WO_3$ in the mixtures. At 1000 °C, the ART is completed for all the $WO_3$ additions (Table 3; Fig. 1e).

On the contrary, when $Nb_2O_5$ is added, no anatase was found in the mixtures fired at 900 °C; the ART polymorphic reaction is fully accomplished. A solid solution between $TiO_2$ and $Nb_2O_5$ is found with 0.01 apfu of $Nb_2O_5$ addition, as in the case of $WO_3$ addition, as the effective ionic radii of $^{[6]}Nb^{4+}$ and $^{[6]}Ti^{4+}$ are 0.68 and 0.61 Å, respectively [33]. With higher $Nb_2O_5$ concentrations (0.025 and 0.05 apfu) there is an excess of $Nb_2O_5$, so that both the end-members of the system are found to coexist (Table 2). With a higher firing temperature, 1000 °C (Table 3), lesser amounts of $Nb_2O_5$ are found as an accessory phase in the mixtures; it can be inferred that $Nb_2O_5$ entered the rutile structure to a higher extent.

Table 2
Phase composition, energy band gap, and specific surface area of the $TiO_2$–REE and $TiO_2$–TM powders fired at 900 °C.

| Sample | Phase composition (wt%) | | | | $E_g$ (eV) | | |
|---|---|---|---|---|---|---|---|
| | Anatase | Rutile | $M$–$TiO_2$ | $M_xO_y$ | Anatase | Rutile | $S_{BET}$ ($m^2\ g^{-1}$) |
| D-900 | – | 100 | – | – | – | $3.03 \pm 0.01$ | 2.0 |
| Ce0.01-900 | – | 98.0 | – | 2.0 | – | $3.07 \pm 0.01$ | 2.1 |
| Ce0.025-900 | – | 94.1 | – | 5.9 | – | $3.08 \pm 0.01$ | 3.3 |
| Eu0.01-900 | – | 98.7 | 1.3 | – | – | $3.06 \pm 0.01$ | 8.6 |
| Eu0.025-900 | – | 91.7 | 8.3 | – | – | $3.06 \pm 0.01$ | 9.1 |
| La0.01-900 | 1.8 | 98.2 | – | – | $3.21 \pm 0.02$ | $3.06 \pm 0.01$ | 11.5 |
| La0.025-900 | – | 88.5 | 11.5 | – | – | $3.06 \pm 0.01$ | 12.0 |
| Y0.01-900 | – | 98.2 | 1.8 | – | – | $3.06 \pm 0.01$ | 8.1 |
| Y0.025-900 | – | 94.8 | 3.9 | 1.4 | – | $3.06 \pm 0.01$ | 8.1 |
| Nb0.01-900 | – | 100 | – | – | – | $3.03 \pm 0.01$ | 3.2 |
| Nb0.025-900 | – | 97.8 | – | 2.2 | – | $3.04 \pm 0.01$ | 4.0 |
| Nb0.05-900 | – | 94.2 | – | 5.8 | – | $3.04 \pm 0.01$ | 5.7 |
| W0.01-900 | 1.3 | 98.7 | – | – | $3.13 \pm 0.02$ | $3.05 \pm 0.01$ | 10.5 |
| W0.025-900 | 15.8 | 82.5 | – | 1.7 | $3.11 \pm 0.01$ | $3.05 \pm 0.01$ | 18.3 |
| W0.05-900 | 17.7 | 75.8 | – | 6.5 | $3.13 \pm 0.02$ | $3.06 \pm 0.01$ | 17.8 |

*Note:* $M$–$TiO_2$ represents the intermediate REE–titanium oxides that are: $Eu_2Ti_2O_7$, $La_4Ti_9O_{24}$, and $Y_2Ti_2O_7$.
$M_xO_y$ represents the TM or REE oxide end-member used in the $TiO_2$–TM and $TiO_2$–REE systems.

Table 3
Phase composition, energy band gap, and specific surface area of the $TiO_2$–REE and $TiO_2$–TM powders fired at 1000 °C.

| Sample | Phase composition (wt%) | | | $E_g$ (eV) | |
|---|---|---|---|---|---|
| | Rutile | $M$–$TiO_2$ | $M_xO_y$ | Rutile | $S_{BET}$ ($m^2\ g^{-1}$) |
| D-1000 | 100 | – | – | $3.01 \pm 0.01$ | 0.5 |
| Ce0.01-1000 | 98.0 | – | 2.0 | $3.04 \pm 0.01$ | < 0.1 |
| Ce0.025-1000 | 94.8 | – | 5.2 | $3.05 \pm 0.01$ | 0.4 |
| Eu0.01-1000 | 96.6 | 3.4 | – | $3.04 \pm 0.01$ | 2.8 |
| Eu0.025-1000 | 91.2 | 8.8 | – | $3.04 \pm 0.01$ | 3.1 |
| La0.01-1000 | 94.8 | 5.2 | – | $3.05 \pm 0.01$ | 4.6 |
| La0.025-1000 | 88.4 | 11.6 | – | $3.05 \pm 0.01$ | 4.4 |
| Y0.01-1000 | 97.6 | 2.4 | – | $3.03 \pm 0.01$ | 2.2 |
| Y0.025-1000 | 93.8 | 5.6 | 0.6 | $3.03 \pm 0.01$ | 2.3 |
| Nb0.01-1000 | 100 | – | – | $3.02 \pm 0.01$ | 0.9 |
| Nb0.025-1000 | 98.6 | – | 1.4 | $3.02 \pm 0.01$ | 0.4 |
| Nb0.05-1000 | 96.9 | – | 3.1 | $3.03 \pm 0.01$ | 1.3 |
| W0.01-1000 | 100 | – | – | $3.03 \pm 0.01$ | 6.0 |
| W0.025-1000 | 94.9 | – | 5.1 | $3.03 \pm 0.01$ | 4.2 |
| W0.05-1000 | 88.4 | – | 11.6 | $3.05 \pm 0.01$ | 4.3 |

*Note*: $M$–$TiO_2$ represents the intermediate REE–titanium oxides that are: $Eu_2Ti_2O_7$, $La_4Ti_9O_{24}$, and $Y_2Ti_2O_7$.
$M_xO_y$ represents the TM or REE oxide end-member used in the $TiO_2$–TM and $TiO_2$–REE systems.

We therefore deem that the miscibility of these TM elements ($WO_3$ and $Nb_2O_5$) and titania is limited to 1 mol%.

### 3.1.1. X-ray diffraction: rare earth element addition

The addition of REE accelerated the ART at both firing temperatures, because of the formation of oxygen vacancies, due to their valence $< 4+$ [31]. The only exception was sample La0.01 fired at 900 °C (Fig. 1f), that also contained a small amount of anatase (1.8 wt% and 98.2 wt% of rutile, Table 2). Moreover – still excluding sample La0.01-900 – no solid solution was found to exist between the REE and $TiO_2$. This is due to the significant differences between the effective ionic radii of the REE, compared to that of $Ti^{4+}$ ($^{[6]}Ce^{4+} = 0.87$ Å, $^{[6]}Eu^{3+} = 0.95$ Å, $^{[6]}La^{3+} = 1.03$ Å, $^{[6]}Y^{3+} = 0.90$ Å, $^{[6]}Ti^{4+} = 0.61$ Å [33]). At both temperatures (Tables 2 and 3), $Eu_2O_3$, $Y_2O_3$, and $La_2O_3$ reacted with $TiO_2$ to form REE–titanium oxides ($Eu_2Ti_2O_7$ and $Y_2Ti_2O_7$ – both having pyrochlore structure – and $La_4Ti_9O_{24}$, respectively), in good agreement with the respective phase diagrams [34–36]. In the system $TiO_2$–$Y_2O_3$, together with rutile and the $Y_2Ti_2O_7$

intermediate, there was also the other end-member, $Y_2O_3$, that did not react with $TiO_2$. At a higher temperature, 1000 °C, the amount of $Y_2O_3$ decreased, with greater $Y_2Ti_2O_7$ formation. In the $TiO_2$–$CeO_2$ system, there were no reactions between the two end-members, at both the tested temperatures, as shown in Tables 2 and 3.

### 3.2. Optical spectroscopy

The DRS spectra of undoped Aeroxide P25 titania powder at RT and fired at 900 and 1000 °C, are depicted in Fig. 2. The thermal treatment, besides completing the ART, also shifted the Aeroxide P25 optical absorption edge to lower energies, consistent with its phase composition. The DRS spectra of the doped powders, thermally treated at 900 °C and 1000 °C, are shown in Figs. 3 and 4. All the doped powders showed a slight shift of their absorption edge into the visible region, due to the presence of rutile. At 900 °C, their DRS spectra can be split into two groups (Fig. 3): Ce–$TiO_2$ and Nb–$TiO_2$, in which the titania absorption edge has a greater shift toward the visible region, and the other group (Eu–, La–, Y–, and W–$TiO_2$). Moreover, Ce–$TiO_2$ sample showed a tail in the visible region of the spectrum, that extends up to ~450 nm, due to the contribution of the free $CeO_2$ in that sample [37]. At 1000 °C, Fig. 4, only the Ce–$TiO_2$ showed a noticeable shift of its absorption edge into the visible region, keeping the tail, at around 450 nm.

The $E_g$s of the powders were calculated by the differential reflectance method (Tables 1–3 and Fig. 5), from an average of three measurements for each sample. The resulting curves were successfully fitted with a Gaussian function (OriginPro Lab, version 8.5), and the maximum values, together with the experimental errors, were calculated from the fitting. Considering the $E_g$ of the powders fired at 900 °C, the $E_g$ of anatase in sample La0.01-900 (3.21 eV) is consistent with the expected value for anatase.

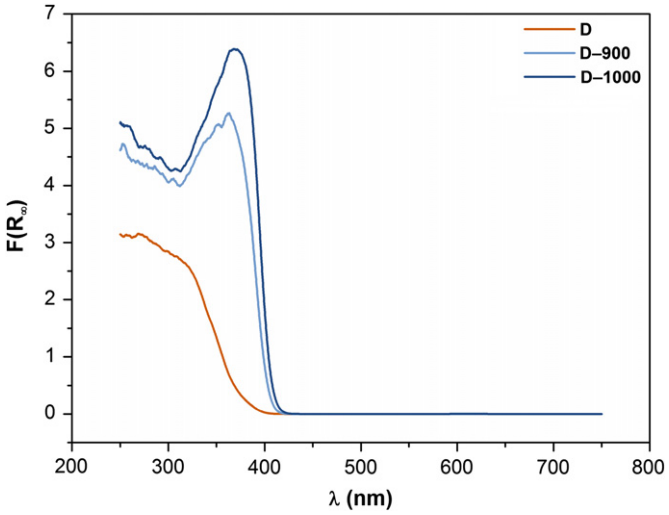


Fig. 2. Diffuse reflectance spectra of Degussa P25 powder at RT (D), fired at 900 °C (D-900) and 1000 °C (D-1000).

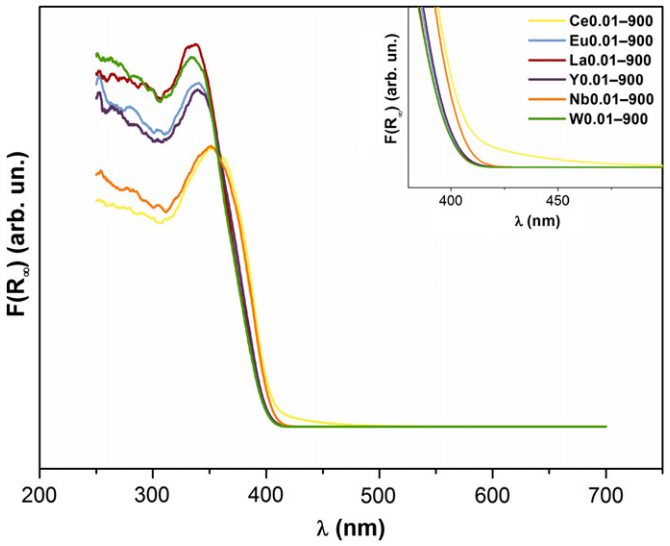


Fig. 3. Diffuse reflectance spectra of $TiO_2$–REE and $TiO_2$–TM mixtures fired at 900 °C. Inset: magnification, in the $\lambda$ range of 350–450 nm, of the reported spectra in order to emphasise their absorption edge into the visible region.

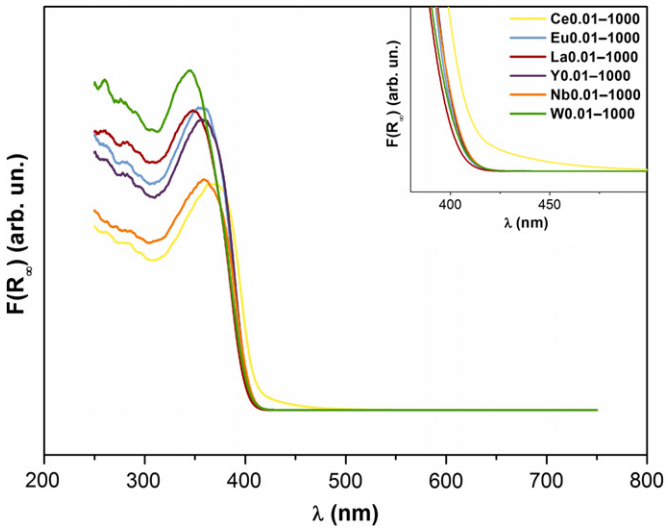


Fig. 4. Diffuse reflectance spectra of $TiO_2$–REE and $TiO_2$–TM mixtures fired at 1000 °C. Inset: magnification, in the $\lambda$ range of 375–475 nm, of the reported spectra in order to emphasise their absorption edge into the visible region.

The $E_g$ of rutile, in the $TiO_2$–REE mixtures, was greater than that of the Aeroxide P25, fired at the same temperature (Table 2); the $E_g$ of rutile in $TiO_2$–TM samples was red-shifted, compared to that of $TiO_2$–REEs. Samples where the solid solution was found (Nb0.01-900 and W0.01-900) possess the lowest $E_g$ of all the $TiO_2$–TM set ($E_g$=3.03 and 3.05 eV, respectively). The presence of the two end-members, in the $TiO_2$–TM mixtures led to an increase of the respective rutile $E_g$ values. The band gap value of anatase in the W–$TiO_2$ samples (3.13 eV) showed a red-shift, if compared to the expected anatase value of 3.20 eV, this is probably due to the incorporation of $WO_3$ into the titania lattice. These latter samples have also a

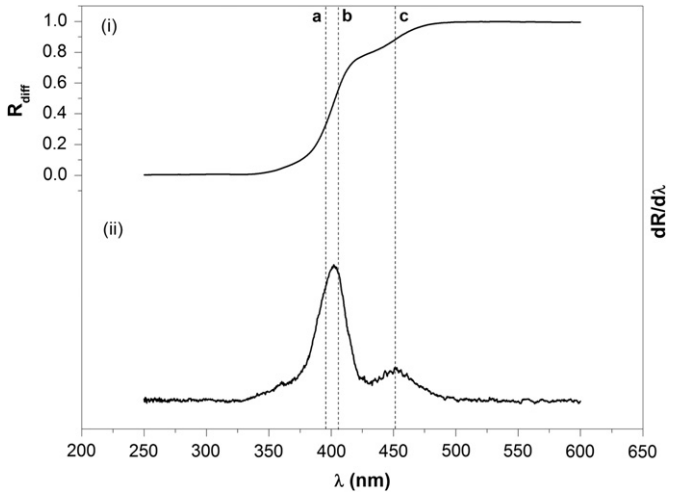


Fig. 5. Diffuse reflectance spectrum of the sample W0.05-900 (i) and first derivative (ii), as function of wavelength $\lambda$. The vertical dashed lines a, b, and c refer to: anatase, rutile, and $WO_3$ $E_g$, respectively.

contribution at approximately 2.75 eV – assigned to the residual $WO_3$ end-member – as shown in the differential reflectance $dR/d\lambda$ Vs wavelength plot, depicted in Fig. 5. Firing at a higher temperature, 1000 °C, caused a decrease – hence a red-shift – of the $E_g$ of rutile in all the samples (Table 3). The $E_g$ of all these samples was within the visible-range. Among the $TiO_2$–REE mixtures, the sample with $Y_2O_3$ addition was the one with the greatest red-shift ($E_g$=3.03 eV). Of the $TiO_2$–TM series, the ones where the solid solution was accomplished are those with the higher red-shift (sample Nb0.01 has a $E_g$=3.02 eV, while sample W0.01 has a $E_g$=3.03 eV).

### 3.3. Photocatalytic activity

The photocatalytic activity results – both in liquid–solid and gas–solid phases – of the powders fired at 900 and 1000 °C, are shown in Fig. 6a–d and in Tables 4 and 5. Since liquid–solid and gas–solid phase results are not directly comparable – different target pollutants in a different phase and at a different initial concentrations; different initial amounts of photocatalyst; different lamps used – they will be discussed separately.

#### 3.3.1. Liquid–solid phase

We considered the MB photolysis to be negligible in the liquid–solid phase photocatalytic experiments, the $\xi$ values being equal to ~3% and ~1%, under UVA and visible-light exposure, respectively, and after 7 h of irradiation time (Fig. 6a and b). Taking into consideration the liquid–solid phase photocatalytic activity of the powders fired at 900 °C (Fig. 6a and Table 4), the reference sample (D-900) possesses an appreciable photocatalytic activity, under UVA-light exposure, degrading almost all the MB used as a target pollutant ($\xi$=97%). Between the $TiO_2$–REE set of samples, the best performing samples under UVA-light irradiation are those where $Y_2O_3$ was added, reaching an extent of photocatalytic degradation $\xi$ of 94% and 97%, for Y0.01-900 and Y0.025 samples, respectively. Actually, these samples, even if the titania phase is rutile, have a low fraction of $Y_2Ti_2O_7$ (namely 1.8 and 3.9 wt%, Table 2), and a rather high SSA (8.1 $m^2 g^{-1}$), this being a factor that favours photocatalytic activity. The addition of the other REE oxides gives rise to samples with a lower photocatalytic activity, compared to the reference one. The activity of such samples, followed the trend Eu > La > Ce, consistent with the SSA of the samples. Considering the $TiO_2$–TM set of samples, their overall photocatalytic activity is lower than the reference sample. The Nb–$TiO_2$ activity increases with the $Nb_2O_5$ amount in the mixture (a solid solution existing for the sample with 1 mol% of $Nb_2O_5$ addition only), suggesting a synergic effect of the two end-members on the photocatalytic activity. It is known that $Nb_2O_5$ is a wide band gap semiconductor ($E_g$=3.4 eV), and possesses a wide range of catalytic activities [38]; the best performing sample was sample Nb0.05-900 ($\xi$=92%) that contains 94.2 wt% of rutile and 5.8 wt% of $Nb_2O_5$. Tungsten addition did not improve the photocatalytic activity of the samples, despite the higher anatase amounts in the mixture, as well as their higher SSA, if compared to the reference sample. This behaviour can be explained by taking into account the relative MB concentration during the reactions. In Fig. 7, it can be seen that when increasing the amount of $WO_3$ in the mixtures, the initial MB adsorption onto these samples increases. Hence, we deem that the high adsorption of MB, on the surface of the powders, overtook their photocatalytic activity.

The thermal treatment at 1000 °C generally led to little change in or a slight decrease of the photocatalytic activity of the samples in liquid–solid phase (Fig. 6b and Table 5). The reference sample still had a reasonable activity ($\xi$=81%), while between the $TiO_2$–REE samples, the Eu-, La-, and Y-doped titanias maintained the performance obtained at 900 °C, degrading almost all the MB, after 7 h of irradiation time. This is because, according to some authors [39,40], those REEs efficiently promote the separation of the photo-generated $e^-$–$h^+$ pairs, hence improving the photocatalytic performance of $TiO_2$. Amongst the $TiO_2$–TM, also in case of the thermal treatment at 1000 °C, samples with $Nb_2O_5$ addition were the best performing ones.

The photocatalytic activity of all the samples decreased under visible-light irradiation. At 900 °C, the reference sample has an extent of MB degradation $\xi$ equal to 38%, owing to the presence of rutile; its band gap is slightly shifted into the visible region (3.03 eV; 409 nm). Amongst the $TiO_2$–REE samples, the best performing ones are the Y–$TiO_2$, degrading 53% of MB. Aside from these samples, the other $TiO_2$–REEs (Eu– and La–$TiO_2$) possess a rather low photocatalytic activity in liquid–solid regime for degrading MB under visible-light exposure, despite their energy band-gaps (3.06 eV; 405 nm) and their SSAs are comparable. Finally, even though the Ce–$TiO_2$ samples

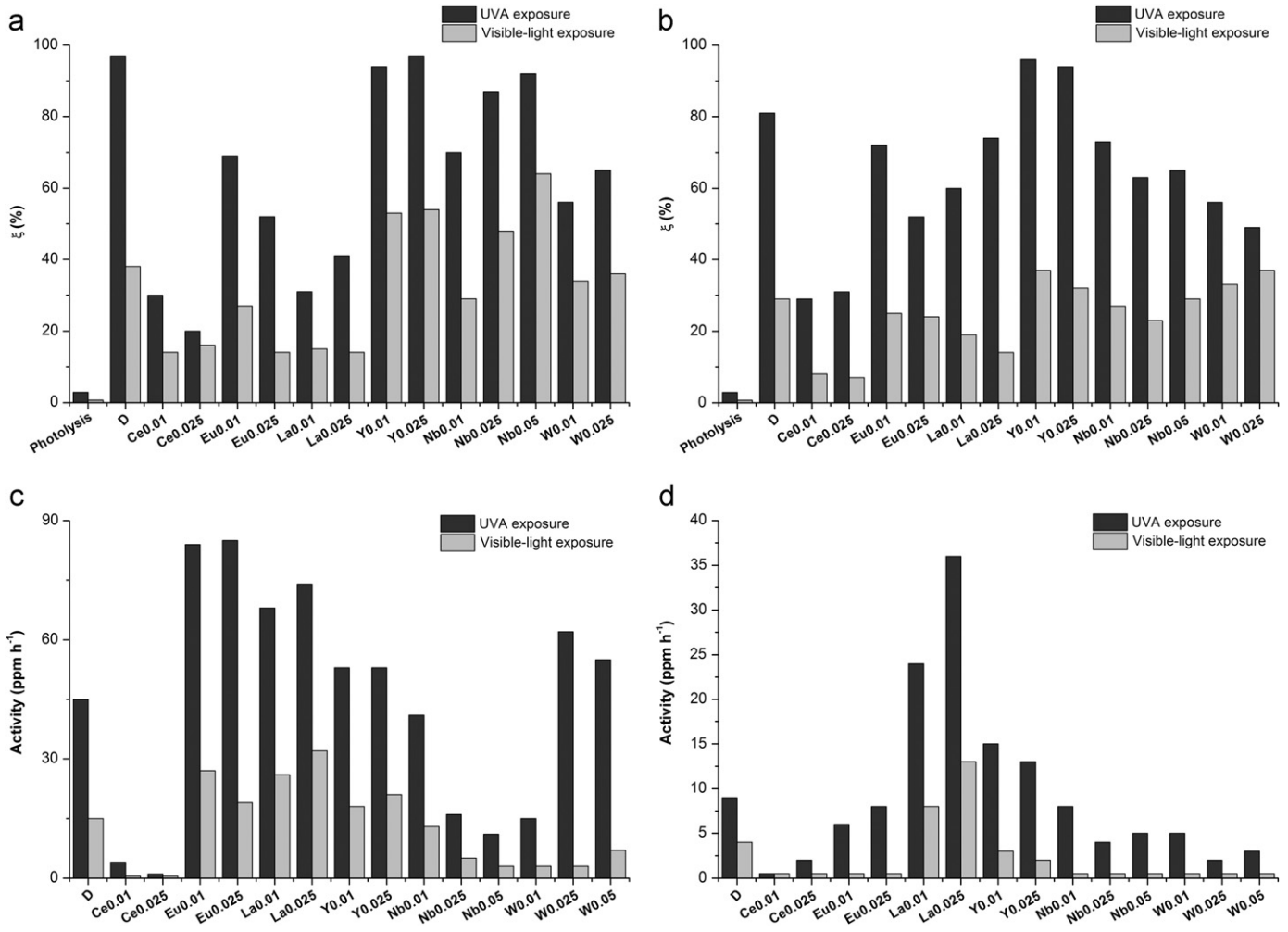


Fig. 6. Photocatalytic activity in liquid–solid phase of: (a) samples fired at 900 °C and (b) samples fired at 1000 °C. In gas–solid phase of: (c) samples fired at 900 °C and (d) samples fired at 1000 °C.

have an absorption tail in the visible region, their photocatalytic activity is the lowest within all the set of samples, because of their low SSA, detrimental for the photocatalytic efficiency. The addition of $WO_3$ did not improve the photocatalytic activity of the samples, compared to the reference one. On the contrary, $Nb_2O_5$ additions ($\geq 0.025$ apfu) gave the samples better degradation performances, in liquid–solid phase conditions, with better results with higher levels of Nb. With a higher thermal treatment at 1000 °C, all the samples were shown to have less photocatalytic activity, due to the decreasing SSA, and an increase of the particle size. Amongst the REE-doped samples, the Y-doped samples were the best performing ones. Of the TM-doped samples, the W-doped samples were the ones with a higher photocatalytic activity, showing greater activity than the Nb-doped samples when calcined at 1000 °C (Table 5).

### 3.3.2. Gas–solid phase

The results of the gas–solid phase reactions are depicted in Fig. 6c–d and in Tables 4 and 5. A typical example of the gas–solid phase photocatalytic experiment is reported in Fig. 8. As can be seen in the inset of Fig. 8, there is no acetone formation prior the irradiation, whilst the slight isopropanol variation does not seem to have any correlation with the method employed to evaluate the photocatalytic activity of the samples. In the gas–solid phase reactions, we observe a markedly different behaviour. At 900 °C, under UVA-light irradiation (Fig. 6c and Table 4), the reference sample still had a good photocatalytic activity (45 ppm $h^{-1}$ of acetone formation). The $TiO_2$–REE samples, with the exception of Ce–$TiO_2$, display a better photocatalytic activity compared to the reference one (Eu > La > Y, refer to Table 4). This is consistent with their SSAs: samples having SSA greater than D-900 have a higher photocatalytic activity. Ce–$TiO_2$ – the samples with the lower SSA – are also the samples with a lower photocatalytic activity in gas–solid phase regime, from monitoring the isopropanol degradation/acetone formation. $TiO_2$–TM samples mostly have a lower photocatalytic activity, compared to the reference one. Exceptions are the samples with 2.5 and 5 mol% of $WO_3$ (62 and 55 ppm $h^{-1}$ of acetone formation) that are the samples with the higher anatase amount in the mixture (15.8 and

Table 4
Photocatalytic activity in liquid– and gas–solid phase of the $TiO_2$–REE and $TiO_2$–TM powders fired at 900 °C.

| Sample | Activity under UVA exposure | | | | Activity under visible-light exposure | | | |
|---|---|---|---|---|---|---|---|---|
| | Liquid–solid phase | | | Gas–solid phase | Liquid–solid phase | | | Gas–solid phase |
| | $\xi$ (%) | $k'_{app}$ ($h^{-1}$) | $R^2$ | Acetone formation (ppm × $h^{-1}$) | $\xi$ (%) | $k'_{app}$ ($h^{-1}$) | $R^2$ | Acetone formation (ppm × $h^{-1}$) |
| D-900 | 97 | 0.550 | 0.995 | 45 | 38 | 0.069 | 0.991 | 15 |
| Ce0.01-900 | 30 | 0.051 | 0.994 | 4 | 14 | 0.027 | 0.931 | < 0.5 |
| Ce0.025-900 | 20 | 0.030 | 0.985 | 1 | 16 | 0.027 | 0.951 | < 0.5 |
| Eu0.01-900 | 69 | 0.172 | 0.995 | 84 | 27 | 0.045 | 0.961 | 27 |
| Eu0.025-900 | 52 | 0.111 | 0.980 | 85 | 14 | 0.023 | 0.958 | 19 |
| La0.01-900 | 31 | 0.057 | 0.983 | 68 | 15 | 0.026 | 0.919 | 26 |
| La0.025-900 | 41 | 0.074 | 0.991 | 74 | 14 | 0.020 | 0.982 | 32 |
| Y0.01-900 | 94 | 0.374 | 0.993 | 53 | 53 | 0.116 | 0.964 | 18 |
| Y0.025-900 | 97 | 0.477 | 0.981 | 53 | 54 | 0.112 | 0.998 | 21 |
| Nb0.01-900 | 70 | 0.170 | 0.998 | 41 | 29 | 0.049 | 0.998 | 13 |
| Nb0.025-900 | 87 | 0.277 | 0.987 | 16 | 48 | 0.095 | 0.985 | 5 |
| Nb0.05-900 | 92 | 0.341 | 0.990 | 11 | 64 | 0.155 | 0.981 | 3 |
| W0.01-900 | 56 | 0.111 | 0.985 | 15 | 34 | 0.060 | 0.997 | 3 |
| W0.025-900 | 65 | 0.136 | 0.979 | 62 | 36 | 0.065 | 0.975 | 3 |
| W0.05-900 | 66 | 0.154 | 0.998 | 55 | 29 | 0.037 | 0.939 | 7 |

Table 5
Photocatalytic activity in liquid– and gas–solid phase of the $TiO_2$–REE and $TiO_2$–TM powders fired at 1000 °C.

| Sample | Activity under UVA exposure | | | | Activity under visible-light exposure | | | |
|---|---|---|---|---|---|---|---|---|
| | Liquid–solid phase | | | Gas–solid phase | Liquid–solid phase | | | Gas–solid phase |
| | $\xi$ (%) | $k'_{app}$ ($h^{-1}$) | $R^2$ | Acetone formation (ppm × $h^{-1}$) | $\xi$ (%) | $k'_{app}$ ($h^{-1}$) | $R^2$ | Acetone formation (ppm × $h^{-1}$) |
| D-1000 | 81 | 0.243 | 0.990 | 9 | 29 | 0.048 | 0.987 | 4 |
| Ce0.01-1000 | 29 | 0.047 | 0.970 | < 0.5 | 8 | 0.011 | 0.968 | < 0.5 |
| Ce0.025-1000 | 31 | 0.055 | 0.991 | 2 | 7 | 0.010 | 0.988 | < 0.5 |
| Eu0.01-1000 | 72 | 0.191 | 0.985 | 6 | 25 | 0.040 | 0.972 | < 0.5 |
| Eu0.025-1000 | 52 | 0.109 | 0.979 | 8 | 24 | 0.040 | 0.981 | < 0.5 |
| La0.01-1000 | 60 | 0.139 | 0.963 | 24 | 19 | 0.031 | 0.997 | 8 |
| La0.025-1000 | 74 | 0.197 | 0.997 | 36 | 14 | 0.021 | 0.986 | 13 |
| Y0.01-1000 | 96 | 0.457 | 0.996 | 15 | 37 | 0.068 | 0.988 | 3 |
| Y0.025-1000 | 94 | 0.410 | 0.998 | 13 | 32 | 0.058 | 0.984 | 2 |
| Nb0.01-1000 | 73 | 0.186 | 0.997 | 8 | 27 | 0.047 | 0.989 | < 0.5 |
| Nb0.025-1000 | 63 | 0.141 | 0.998 | 4 | 23 | 0.039 | 0.983 | < 0.5 |
| Nb0.05-1000 | 65 | 0.135 | 0.960 | 5 | 29 | 0.050 | 0.993 | < 0.5 |
| W0.01-1000 | 56 | 0.114 | 0.992 | 5 | 33 | 0.060 | 0.978 | < 0.5 |
| W0.025-1000 | 49 | 0.094 | 0.991 | 2 | 37 | 0.071 | 0.983 | < 0.5 |
| W0.05-1000 | 53 | 0.102 | 0.979 | 3 | 30 | 0.049 | 0.982 | < 0.5 |

17.7 wt%, respectively). At 1000 °C, the photocatalytic activity of the samples greatly decreased (Fig. 6d). Exceptions were the La– and Y–$TiO_2$ that kept a reasonably high photocatalytic activity, greater than that of the reference sample, despite the thermal treatment at a temperature of 1000 °C.

The visible-light exposure in gas–solid phase led to a decrease of the photocatalytic activity of all the samples. Amongst the $TiO_2$–REE samples, Eu–, La–, and Y–$TiO_2$ still have excellent photocatalytic performances, due to their high SSAs, and consequently, reduced particle size. The best photocatalysts, under visible-light irradiation, are the La– and Eu–$TiO_2$. Hence, considering that system (gas–solid phase, visible-light exposure, and isopropanol degradation/acetone formation), the mixing of those REEs in the rutile structure improved its visible-light photocatalytic activity.

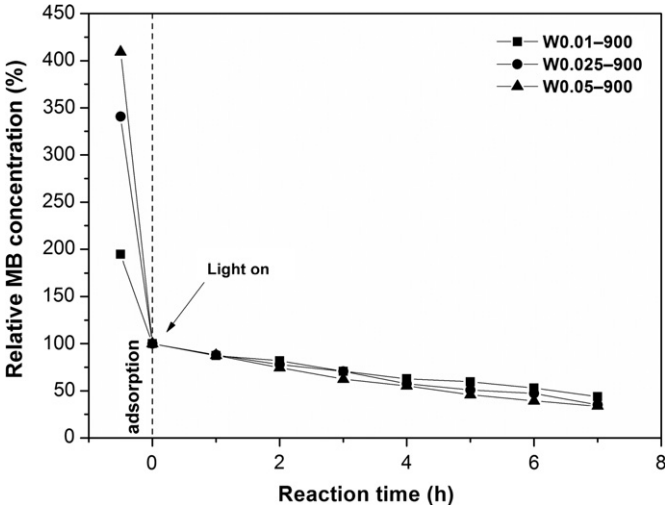


Fig. 7. Photocatalytic degradation of MB, assessed by W-doped samples fired at 900 °C, in liquid–solid phase and under UVA light exposure.

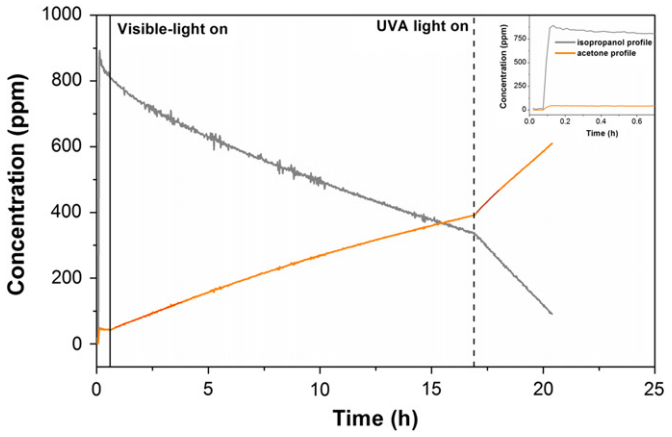


Fig. 8. A typical pattern of the gas–solid phase photocatalytic experiment (sample La0.01-900). The isopropanol profile is in grey and the acetone is in orange. The vertical continuous line represents the time at which the visible-light was turned on; the vertical dashed line represents when the UVA light was turned on. Shown in the inset is a magnification of the isopropanol/ acetone profiles while the reactor was not irradiated, in order to show the absence of acetone in dark conditions. (For interpretation of the references to color in this figure caption, the reader is referred to the web version of this article.)

On the contrary, Ce–$TiO_2$ samples have no photocatalytic activity, consistent with their low SSA. $TiO_2$–TMs have a lower photocatalytic activity, compared to the reference sample, the only exception being sample Nb0.01-900, whose photocatalytic activity is comparable to the reference sample. The thermal treatment at 1000 °C led to a disappearance of the photocatalytic activity for all the $TiO_2$–TMs, and for most of the $TiO_2$–REEs. The only samples that retained a degree of photocatalytic activity at this firing temperature were La–$TiO_2$. According to some authors [41,42], TMs behave as electron-hole recombination centres, whereas on the contrary, REEs – like Eu, La, and Y – are believed to favour the separation of the photo-generated couple $e^-$–$h^+$, and hence, to prevent their recombination [39,40].

## 4. Conclusions

A series of $TiO_2$–TM and $TiO_2$–REE mixtures were prepared via solid-state reaction of the precursor oxides. The products of the synthesis were thermally treated at 900 °C and 1000 °C; their photocatalytic activity was tested both in liquid–solid and in gas–solid phases, under UVA and visible-light exposure. The aim is a possible application on the surface of materials that need treatments at high temperature, so as to give them an innovative surface functionalisation.

The addition of $WO_3$ to titania shifted the ART to a higher temperature; on the contrary, when $Nb_2O_5$ was added, the ART polymorphic reaction was already fully accomplished at 900 °C. The addition of REE accelerated the ART, at both firing temperatures, because of the formation of oxygen vacancies. The only exception was the sample with 0.01 apfu of La, fired at 900 °C, that also contained a small amount of anatase (1.8 wt%).

From the DRS spectra, all the doped powders – fired at both firing temperatures – showed a slight shift of their absorption edge into the visible region, due to the presence of rutile.

Photocatalytic activity results in liquid–solid and gas–solid phases were not directly comparable. In the liquid–solid phase photocatalytic tests, Y-doped and Nb-doped samples were shown to be the most promising photocatalysts, at both the firing temperatures and with both the light exposures (UVA and visible). In the gas phase tests, Eu-, La-, and Y-doped powders, were the most active samples, both under UVA and visible-light irradiation at 900 °C, showing them to be the most suitable for an exterior application. On the other hand, when the thermal treatment was at 1000 °C, this was detrimental for their photocatalytic activity.

## Acknowledgements

R.C. Pullar and M.P. Seabra wish to thank the FCT Ciencia2008 Programme for supporting this work. D.M. Tobaldi gratefully acknowledge the FCT for the financial support (Grant BPD/UI89/5681/2012).

## References

[1] J. Chen, C.-S. Poon, Photocatalytic construction and building materials: from fundamentals to applications, Building and Environment 44 (2009) 1899–1906.
[2] F. Chen, X. Yang, H.K.C. Mak, D.W.T. Chan, Photocatalytic oxidation for antimicrobial control in built environment: A brief literature overview, Building and Environment 45 (2010) 1747–1754.
[3] V. Puddu, H. Choi, D.D. Dionysiou, G. Li Puma, $TiO_2$ photocatalyst for indoor air remediation: influence of crystallinity, crystal phase, and UV radiation intensity on trichloroethylene degradation, Applied Catalysis B: Environmental 94 (2010) 211–218.
[4] S. Malato, P. Fernández-Ibáñez, M.I. Maldonado, J. Blanco, W. Gernjak, Decontamination and disinfection of water by solar photocatalysis: recent overview and trends, Catalysis Today 147 (2009) 1–59.

[5] A. Fujishima, T.N. Rao, D.A. Tryk, Titanium dioxide photocatalysis, Journal of Photochemistry and Photobiology C: Photochemistry Reviews 1 (2000) 1–21.
[6] A. Fujishima, X. Zhang, D.A. Tryk, $TiO_2$ photocatalysis and related surface phenomena, Surface Science Reports 63 (2008) 515–582.
[7] M.R. Hoffmann, S.T. Martin, W. Choi, D.W. Bahnemann, Environmental application of semiconductor photocatalysis, Chemical Reviews 95 (1995) 69–96.
[8] F. Arsac, D. Bianchi, J.M. Chovelon, P. Conchon, C. Ferronato, A. Lair, M. Sleiman, Photocatalytic degradation of organic pollutants in water and in air. An analytical approach, Materials Science and Engineering **C** 28 (2008) 722–725.
[9] J.-M. Herrmann, C. Duchamp, M. Karkmaz, B.T. Hoai, H. Lachheb, E. Puzenat, C. Guillard, Environmental green chemistry as defined by photocatalysis, Journal of Hazardous Materials 146 (2007) 624–629.
[10] S. Sakthivel, H. Kisch, Daylight photocatalysis by carbon-modified titanium dioxide, Angewandte Chemie-International Edition 42 (2003) 4908–4911.
[11] J.C. Yu, J.G. Yu, W.K. Ho, Z.T. Jiang, L.Z. Zhang, Effects of F—doping on the photocatalytic activity and microstructures of nanocrystalline $TiO_2$ powders, Chemistry of Materials 14 (2002) 3808–3816.
[12] T. Umebayashi, T. Yamaki, S. Tanaka, K. Asai, Visible light-induced degradation of methylene blue on S-doped $TiO_2$, Chemistry Letters 32 (2003) 330–331.
[13] X. Hong, Z. Wang, W. Cai, F. Lu, J. Zhang, Y. Yang, N. Ma, Y. Liu, Visible-light-activated nanoparticle photocatalyst of iodine-doped titanium dioxide, Chemistry of Materials 17 (2005) 1548–1552.
[14] R. Asahi, T. Morikawa, T. Ohwaki, Y. Taga, Visible-light photocatalysis in nitrogen-doped titanium oxides, Science 293 (2001) 269–271.
[15] M. Anpo, Use of visible light. Second-generation titanium oxide photocatalysts prepared by the application of an advanced metal ion-implantation method, Pure and Applied Chemistry 72 (2000) 1702–1787.
[16] M.A. Rauf, M.A. Meetani, S. Hisaindee, An overview on the photocatalytic degradation of azo dyes in the presence of $TiO_2$ doped with selective transition metals, Desalination 276 (2011) 13–27.
[17] A.-W. Xu, Y. Gao, H.-Q. Liu, The preparation, characterization, and their photocatalytic activities of rare-earth-doped $TiO_2$ nanoparticles, Journal of Catalysis 207 (2002) 151–157.
[18] J. Li, X. Yang, X. Yu, L. Xu, W. Kang, W. Yan, H. Gao, Z. Liu, Y. Guo, Rare earth oxide-doped titania nanocomposites with enhanced photocatalytic activity towards the degradation of partially hydrolysis polyacrylamide, Applied Surface Science 255 (2009) 3731–3738.
[19] X. Zhang, K. Udagawa, Z. Liu, S. Nishimoto, C. Xu, Y. Liu, H. Sakai, M. Abe, T. Murakami, A. Fujishima, Photocatalytic and photoelectrochemical studies on N-doped $TiO_2$ photocatalyst, Journal of Photochemistry and Photobiology A: Chemistry 202 (2009) 39–47.
[20] M. Kitano, K. Funatsu, M. Matsuoka, M. Ueshima, M. Anpo, Preparation of nitrogen-substituted $TiO_2$ thin film photocatalysts by the radio frequency magnetron sputtering deposition method and their photocatalytic reactivity under visible light irradiation, Journal of Physical Chemistry 110 (2006) 25266–25272B 110 (2006) 25266–25272.
[21] D.M. Tobaldi, A. Tucci, G. Camera–Roda, G. Baldi, L. Esposito, Photocatalytic activity for exposed building materials, Journal of the European Ceramic Society 28 (2008) 2645–2652.
[22] M.P. Seabra, R.R. Pires, J.A. Labrincha, Ceramic tiles for photodegradation of Orange II solutions, Chemical Engineering Journal 171 (2011) 692–702.
[23] R.A. Spurr, H. Myers, Quantitative analysis of anatase–rutile mixtures with an X-ray diffractometer, Analytical Chemistry 29 (1957) 760–762.
[24] R.L. Snyder, X-ray diffraction, in: E. Lifshin (Ed.), X-ray Characterization of Materials, Wiley–VCH, New York, 1999, pp. 1–104.
[25] A.S. Marfunin, Physics of minerals and inorganic materials. An introduction, Springer–Verlag, Berlin, 1979.
[26] M. Radecka, M. Rekas, K. Zakrzewska, Titanium dioxide in photoelectrolysis of water, Trends in Inorganic Chemistry 9 (2006) 81–126.
[27] H. Al-Ekabi, N. Serpone, Kinetics studies in heterogeneous photocatalysis. I. Photocatalytic degradation of chlorinated phenols in aerated aqueous solutions over titania supported on a glass matrix, Journal of Physical Chemistry 92 (1988) 5726–5731.
[28] M. Tasbihi, U. Lavrenčič Štangar, A. Sever Škapin, A. Ristić, V. Kaučič, N. Novak Tušar, Titania-containing mesoporous silica powders: structural properties and photocatalytic activity towards isopropanol degradation, **J**ournal of Photochemistry and Photobiology A: Chemistry 216 (2010) 167–178.
[29] D.M. Tobaldi, A. Tucci, A. Sever Škapin, L. Esposito, Effects of $SiO_2$ addition on $TiO_2$ crystal structure and photocatalytic activity, Journal of the European Ceramic Society 30 (2010) 2481–2490.
[30] S.A. Larson, J.A. Widergren, J.L. Falconer, Transient studies of 2-propanol photocatalytic oxidation on titania, Journal of Catalysis 157 (1995) 611–625.
[31] R.D. Shannon, J.A. Pask, Kinetics of the anatase-rutile transformation, Journal of the American Ceramic Society 48 (1965) 391–398.
[32] K. Okada, N. Yamamoto, Y. Kameshima, A. Yasumori, K.J.D. MacKenzie, Effect of silica additive on the anatase-to-rutile phase transition, Journal of the American Ceramic Society 84 (2001) 1591–1596.
[33] R.D. Shannon, Revised effective ionic radii and systematic studies of interatomic distances in halides and chalcogenides, Acta crystallographica A32 (1976) 751–767.
[34] B. Iwasaki, System $Eu_2O_3$-$TiO_2$ in air (subsolidus), Bulletin of the Chemical Society of Japan 51 (1978) 3223–3226.
[35] N. Mizutani, Y. Tajima, M. Kato, Phase relations in the system $Y_2O_3$-$TiO_2$, Journal of the American Ceramic Society 59 (1976) 168–168.
[36] S.D. Škapin, D. Kolar, D. Suvorov, Phase stability and equilibria in the $La_2O_3$–$TiO_2$ system, Journal of the European Ceramic Society 20 (2000) 1179–1185.
[37] F. Galindo-Hernández, R. Gómez, Degradation of the herbicide 2,4-dichlorophenoxyacetic acid over $TiO_2$–$CeO_2$ sol–gel photocatalysts: effect of the annealing temperature on the photoactivity, Journal of Photochemistry and Photobiology A: Chemistry 217 (2011) 383–388.
[38] A.G.S. Prado, L.B. Bolzon, C.P. Pedroso, A.O. Moura, L.L. Costa, $Nb_2O_5$ as efficient and recyclable photocatalyst for indigo carmine degradation, Applied Catalysis B: Environmental 82 (2008) 219–224.
[39] N. Xinshu, L. Sujuan, C. Huihui, Z. Jianguo, Preparation, characterization of $Y^{3+}$-doped $TiO_2$ nanoparticles and their photocatalytic activities for methyl orange degradation, Journal of Rare Earths 29 (2011) 225–229.
[40] S. Huixian, Z. Tianyong, W. Hongliang, Preparation and photocatalytic activity of $La^{3+}$ and $Eu^{3+}$ co-doped $TiO_2$ nanoparticles: photo-assisted degradation of methylene blue, Journal of Rare Earths 29 (2011) 746–752.
[41] N. Serpone, D. Lawless, J. Disdier, J.-M. Herrmann, Spectroscopic, photoconductivity, and photocatalytic studies of $TiO_2$ colloids: naked and with the lattice doped with $Cr^{3+}$, $Fe^{3+}$, and $V^{5+}$ cations, Langmuir 10 (1994) 643–652.
[42] A. Di Paola, E. García-López, S. Ikeda, G. Marcì, B. Ohtani, L. Palmisano, Photocatalytic degradation of organic compounds in aqueous systems by transition metal doped polycrystalline $TiO_2$, Catalysis Today 75 (2002) 87–93.